Energy 63 (2013) 109–122

Contents lists available at ScienceDirect

Energy

journal homepage: www.elsevier.com/locate/energy

Effect of the critical temperature of organic fluids on supercritical pressure Organic Rankine Cycles

Jinliang Xu [a,b,*], Chao Liu [a]

[a] The Beijing Key Laboratory of Multiphase Flow and Heat Transfer, North China Electric Power University, Beijing 102206, PR China
[b] The Beijing Key Laboratory of Renewable and Clean Energy, North China Electric Power University, Beijing 102206, PR China

ARTICLE INFO

Article history:
Received 5 February 2013
Received in revised form
15 September 2013
Accepted 18 September 2013
Available online 7 November 2013

Keywords:
Supercritical pressure ORC (Organic Rankine Cycle)
Critical temperature
Operation parameter
Thermal efficiency
Exergy efficiency

ABSTRACT

The thermal performance of supercritical pressure ORCs (Organic Rankine Cycles) is related to the critical temperature of the organic fluids. The heat source in this investigation was flue gas with an inlet temperature of 150 °C and an outlet temperature of 70 °C. The working fluids were R218, R134a and R236fa. An integrated-average temperature difference was used to quantify the thermal match between the flue gas and the organic fluid in the evaporator. Three types of operating modes were identified: (1) a flexible operating mode for low T_c (critical temperature) fluids having operating states in a rectangular region in a plot of the turbine inlet pressures versus temperatures; (2) a bifurcated operating mode for moderate T_c fluids with one or two pressures corresponding to the turbine inlet temperature; (3) a restricted operating mode for high T_c fluids with only one turbine inlet pressure possible for the turbine inlet temperature. The high T_c organic fluid has a small integrated-average temperature difference that yields large evaporator and system exergy efficiencies. Thus, the useful power is increased. The low T_c organic fluid has a bad thermal match in the evaporator that leads to lower ORC (Organic Rankine Cycle) thermal performance.

1. Introduction

Low grade thermal energy such as waste heat from industrial processes, geothermal heat and heat from low to mid temperature solar collectors, accounts for 50% or more of the total heat generated worldwide [1]. The Organic Rankine Cycle ORC (Organic Rankine Cycle) has been extensively investigated as an efficient means to convert low grade energy into power. Electric power production at low-enthalpy (~150 °C) geothermal sites is usually realized using an ORC process [2]. Hot water with temperatures of 100–200 °C is pumped from rock layers deep within the earth, with the heat transferred in a heat exchanger to a working fluid. The thermal energy is then converted to electricity via a low-temperature cycle. Heberle and Brüggemann [3] considered the option of combined heat and power generation for geothermal resources at temperatures below 450 K. Series and parallel ORC designs and an additional heat generation source were compared based on the second law analysis. Their results showed that the combined heat and power generation significantly increases the second law efficiency of the geothermal power plant in comparison to just power generation alone. The most efficient concept was a series circuit with a high critical temperature organic fluid such as isopentane. For parallel circuits with power generation, fluids such as R227ea with low critical temperatures were preferred. Guo et al. [4] proposed a cogeneration system driven by a low-temperature geothermal source. The system consisted of a low-temperature, geothermally powered ORC subsystem, an intermediate heat exchanger and a commercial R134a heat pump subsystem. Al-Sulaiman et al. [5] performed energy and exergy analyses of a biomass trigeneration system using an ORC. Four cases were considered with electrical power, cooling and cogeneration, heating and cogeneration and trigeneration systems. Their results showed that the best trigeneration system performance was obtained with the lowest ORC evaporator pinch temperature of 20 K and the lowest ORC minimum temperature of 345 K. Alternatively, Hung et al. [6] pointed out that an appropriate combination of solar energy and an ORC system with a higher turbine inlet temperature and a lower condenser temperature (such as deep under sea) provides an economically feasible and environment friendly renewable energy conversion system.

The effects of the working fluid properties on subcritical pressure ORCs have been widely studied in the past. Saleh et al. [7] gave a thermodynamic screening of 31 pure component working fluids for ORCs using the BACKONE equation of state. For the geothermal

* Corresponding author. School of Energy, Power and Mechanical Engineering, North China Electric Power University, Beijing 102206, PR China. Tel./fax: +86 10 61772268.
E-mail address: xjl@ncepu.edu.cn (J. Xu).

0360-5442/$ – see front matter © 2013 Elsevier Ltd. All rights reserved.
http://dx.doi.org/10.1016/j.energy.2013.09.068

Nomenclature

C_p	specific heat (kJ/kg K)
E	exergy (kW)
h	specific enthalpy (kJ/kg)
k	slope or gradient of the T–Q curve (K/kW)
m	mass flow rate (kg/s)
P	pressure (MPa)
Q	heating power (kW)
Q_a	total heat released by flue gas (kW)
s	specific entropy (kJ/kg K)
T	temperature (K)
W	power (kW)

Greek symbols

δ	isentropic pressure difference (MPa)
ΔT	temperature difference between flue gas and organic fluid (°C or K)
η	efficiency

Subscripts

0	reference state
1 ~ 5	points corresponding to Fig. 1
ave	integrated-average
c	critical state of organic fluid
exe	exergy
eva	evaporator
gas	flue gas
in	inlet
M or *M′*	point at which $k_{ORC} = k_{gas}$
max	maximum value
min	minimum value
out	outlet
ORC	Organic Rankine Cycle or organic fluid
p	pinch point or pump
pc	pseudocritical state of organic fluid
r	requirement
s	isentropic
sat	saturation point
sys	ORC system
t	turbine
u	useful
V	the evaporator outlet of organic fluid
water	cooling water

power plants, the ORCs were assumed to operate between 100 and 30 °C and pressures below 2.0 MPa, but in some cases supercritical pressures were also considered. They noted that superheating is not recommended for subcritical pressure ORCs. In the case of superheated vapor at the turbine exit, an internal heat exchanger in the cycle improves the thermal performance.

Lakew and Bolland [8] studied the effects of working fluid properties for low temperature heat sources using a simple ORC. They screened the working fluids based on the power production capability and the component (heat exchanger and turbine) size requirements. Their working fluids were R134a, R123, R227ea, R245fa, R290, and n-pentane. The outputs of the energy balance were used as inputs for the exergy analysis and the component design. R227ea gave the highest power for heat source temperatures of 80–160 °C while R245fa produced the highest for temperatures of 160–200 °C. There was an optimal pressure that minimized the heat exchanger surface area. The optimum pressure was found to be dependent on the heat source temperatures and the working fluids.

Lai et al. [9] investigated the effect of working fluids for high temperature ORCs using alkanes, aromates and linear siloxanes. "Isolated" ORC cycles with maximum temperatures of 250 °C and 300 °C were studied at sub or supercritical pressures. The thermal efficiencies for the different fluids were about 70% of the Carnot efficiency and increased with the critical temperature.

There have been many papers about subcritical pressure ORCs published in the open literature. The key scientific issue is the thermal match between the heat carrier fluid and the organic fluid in the evaporator. A subcritical pressure ORC can have isothermal boiling in the evaporator with a poor thermal match between the heat carrier fluid and the organic fluid [10]. This situation can be improved by a supercritical pressure ORC, in which the organic fluid is directly heated from the liquid state to a supercritical state, bypassing the two-phase region, which gives a better thermal match with the heat source. Thus, the exergy destruction in the evaporator is decreased.

Supercritical pressure ORCs are not yet commercialized, but they have received much attention in recent years. The investigation by Karellas and Schuster [11] showed that the supercritical conditions in ORC applications tend to give promising results in decentralized energy production systems. Cayer et al. [12] analyzed CO_2 transcritical power cycles using an industrial low-grade flue gas as the heat source. The heat source temperature was 100 °C while the mass flow rate was 314.5 kg/s. The maximum and minimum CO_2 temperatures were 95 °C and 15 °C, respectively. The water heat sink was at 10 °C. The methodology included an energy analysis, an exergy analysis, finite size thermodynamics and a heat exchanger surface area analysis. The results gave an optimum high pressure for each of the four steps. Schuster et al. [13] optimized supercritical pressure ORCs for various working fluids in terms of their thermal efficiency and the usable percentage of the heat. The reduction of exergy losses was analyzed based on the need for surplus heat exchanger surface.

Chacartegui et al. [14] proposed supercritical and transcritical CO_2 cycles for solar energy applications. They used a stand-alone closed cycle as well as a topping CO_2 gas turbine and a bottoming ORC. Arslan and Yetik [15] used an ANN (artificial neural network) to optimize a supercritical ORC-binary geothermal power plant. Zhang et al. [16] studied subcritical ORC and transcritical power cycle system for low-temperature geothermal power generation. They showed that R125 in transcritical power cycle gives excellent economic and environmental performance that can maximize the geothermal utilization, which is preferable for a low-temperature geothermal ORC system. R41 provides excellent performance except for its flammability. Baik et al. [17] compared the power production for CO_2 and R125 transcritical cycles for a low grade heat source. Even though the CO_2 cycle had better heat transfer and pressure drop characteristics in the heat exchangers, the high pumping power reduces the cycle's power output. The R125 transcritical cycle was recommended for heat sources of about 100 °C.

Thus, supercritical pressure CO_2 cycles have been investigated for various conditions. The critical temperature of CO_2 is 31.0 °C, which is so low that CO_2 cycles are able to recover heat from heat sources of about 100 °C. However, CO_2 cycles need high pressure of perhaps of 16.0 MPa [10]. The low critical temperature of CO_2 also presents a challenge in condensing the CO_2 vapor in the condenser. Thus, alternative organic fluids should be considered in the near future. Review articles such as Vélez et al. [18], Chen et al. [19] and

Tchanche et al. [20] commented on the important effects of the thermodynamic and physical properties, stability, environmental impact, safety and compatibility, availability and cost when selecting a working fluid.

For a flue gas driven supercritical pressure ORC, the following issues are important:

Coupling of the heat source with the ORC: Previous studies of ORCs considered heat sources with fixed mass flow rates and inlet temperatures of the flue gas [12]. The useful power output ($W_u = W_t - W_p$, where W_t is the turbine power and W_p is the pump power) is related to the thermal efficiency, η, as $W_u = \eta Q_a$, where Q_a is the heat received from the heat source, $Q_a = m_{gas}C_{p,gas}(T_{gas,in} - T_{gas,out})$. Since Q_a can vary due to the variable $T_{gas,out}$, the useful power and thermal efficiency are two independent parameters. A small difference between the inlet and outlet flue gas temperatures means that the waste heat is not fully recovered. In such circumstances, the cycle has a smaller useful power output even though the cycle has a higher thermal efficiency. For practical applications, the waste heat temperature should be decreased as low as possible to maximize the waste heat recovery. This paper presents a method to couple the heat source with the ORC to improve the heat recovery.

Operating parameters: Operating parameters refer to the parameters which can be adjusted to modify the thermal efficiency and power output. The pressures and temperatures at various locations are operating parameters and the mass flow rate of the organic fluid can be changed by adjusting the pump power. Thus, the pressures, temperatures, mass flow rate and pump power are the operating parameters. Little is known about selecting suitable operating parameters for the design, control and operation of supercritical pressure ORCs.

Working fluids for supercritical pressure ORCs: Some organic fluids not including CO_2 are recommended for supercritical pressure ORCs, but little is known on why some fluids provide better thermal performance. More detailed studies are needed to investigate the effects of the working fluid properties on supercritical pressure ORCs.

The objective of this paper is to present a new design method for supercritical pressure ORCs so that the heat source is fully coupled thermodynamically with the ORC. This ensures the largest waste heat recovery degree and maximum useful power. The heat source is characterized by the flue gas mass flow rate and the inlet and outlet flue gas temperatures. This method is then used to investigate the effects of the operating parameters on supercritical pressure ORCs with emphasis on the effect of the critical temperature of the organic fluid on the ORC performance. The study shows a strong connection between the fluid critical temperature and the cycle performance.

2. Problem statement and its solution strategy

2.1. The problem statement

The heat carrier fluid of the heat source can be flue gas, hot water (geothermal energy) and heated oil (solar heat), etc. There is a large amount of flue gas waste heat in industry. Since the flue gas may have water vapor, the waste heat recovery includes sensible heat recovery and latent heat recovery. For the latent heat recovery, the flue gas temperature should be decreased to lower than the dew point temperature so that the latent heat in the vapor in the flue gas can be extracted. This study deals with the sensible heat recovery. In Beijing, about two-thirds of the heat supply in the winter is provided by natural gas boilers [21]. During normal operation, a single natural gas boiler has a flue gas flow rate of about 17t/h (4.7 kg/s) and a temperature of about 150 °C. Extracting the thermal energy from the flue gas will reduce the "thermal-island effect" for the city with a flue gas heat driven ORC as a good technical solution. The aim of this paper is to

1) develop a model to efficiently couple a supercritical pressure ORC with a heat source;
2) use the model to decide operating parameters;
3) analyze the effect of the fluid critical temperature on the supercritical pressure ORC.

Fig. 1a shows an ORC coupled with a heat source. The heat source is characterized by the mass flow rate, m_{gas}, inlet temperature, $T_{gas,in}$, and outlet temperature, $T_{gas,out}$, of the heat carrier fluid which can be flue gas, water, or other fluids. Flue gas is used here as a representative fluid with its physical properties identical to those of dry air at atmospheric pressure. The flue gas transfers heat to the ORC via an evaporator. Fig. 1b shows the T–s diagram for the supercritical pressure ORC. Processes 1–2s is an ideal isentropic expansion while 1–2 is a real non-isentropic expansion. The organic fluid in the condenser passes through a superheated vapor state at point 2, a saturated vapor state at point 3 and a saturated liquid state at point 4.

Neglecting the pressure drops in the evaporator and condenser, there are two pressures in the ORC with a supercritical pressure of $P_5 = P_1 > P_c$ and a subcritical pressure of $P_2 = P_3 = P_4 < P_c$. Usually, the organic fluid is cooled by air or water at the ambient

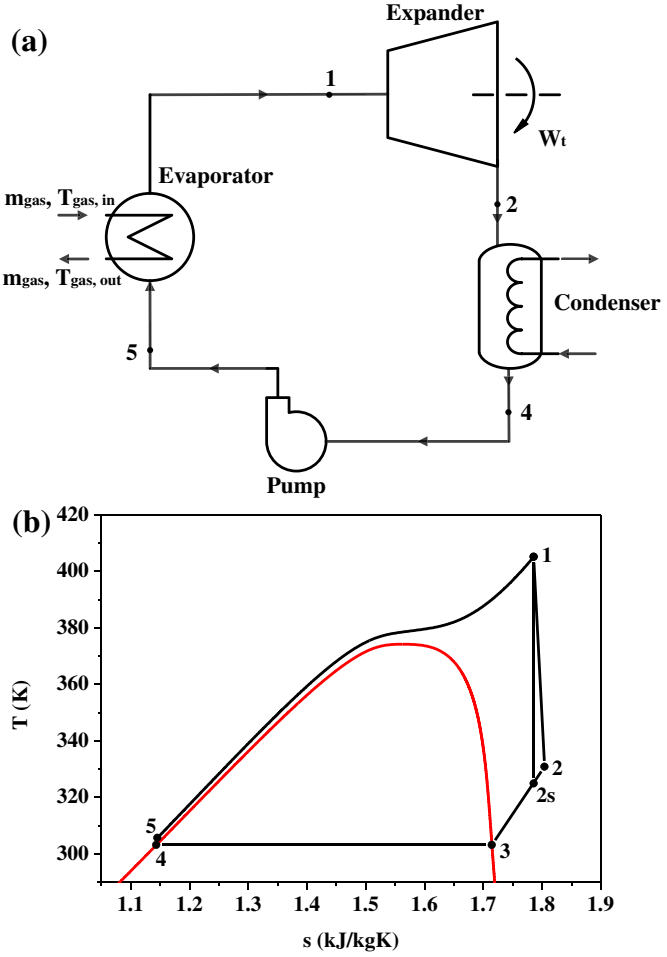

Fig. 1. The basic Organic Rankle Cycle and the T–s diagram for supercritical pressure ORC (the working fluid is R134a, T_c = 374.21 K, P_c = 4.059 MPa, T_1 = 405.15 K, P_1 = 4.458 MPa).

temperature. Thus, the analysis assumes $T_3 = T_4 = 303.15$ K (30 °C). The condensation pressure is $P_2 = P_3 = P_4 = P_{sat}(T_3)$.

The design method will identify suitable operating parameters for the ORC within the constraints of the heat source conditions and the pinch temperature difference in the evaporator. The cycle is simplified by not including an IHE (internal heat exchanger).

2.2. Solution strategy

Since m_{gas}, $T_{gas,in}$ and $T_{gas,out}$ are given, the total heat transferred by the evaporator is

$$Q_a = m_{gas}C_{p,gas}(T_{gas,in} - T_{gas,out}) \quad (1)$$

where $C_{p,gas}$ is the average specific heat of the flue gas based on the temperature $0.5(T_{gas,in} + T_{gas,out})$. Neglecting the specific heat variation with temperature, the heat transfer process follows the linear curve *XY* for the flue gas in Fig. 2. The *XY* line is described by

$$Q = m_{gas}C_{p,gas}(T - T_{gas,out}) \quad (2)$$

The solution strategy consists of two major steps. The first step is to determine a suitable turbine inlet pressure, P_1, for a given turbine inlet temperature, T_1, that matches the heat source and pinch temperature difference constraints. The second step is to determine the cycle operating parameters by changing the turbine inlet temperatures. The following assumptions were made:

Maximum pressure: CO_2 supercritical pressure cycles have been studied in the literature, with pressures up to 16.0 MPa [10]. One objective of this paper is to search for other organic fluids that can be used for supercritical pressure ORCs. Turbines are difficult to be manufactured for high pressures. Therefore, the maximum pressure is assumed to be 10.0 MPa, which is higher than the CO_2 critical pressure of 7.377 MPa.

Pressure difference: The pressure difference is equal to the pressure drop in the turbine with the pressure drops in the other components neglected.

Pinch temperature difference: The required pinch temperature difference in the evaporator is 10.0 K, i.e., $\Delta T_{p,r} = 10.0$ K.

Turbine inlet temperature: The maximum turbine inlet temperature is 10.0 K less than the flue gas inlet temperature by, i.e., $T_{1,max} = T_{gas,in} - 10.0$ K.

Isentropic efficiency: The turbine and pump isentropic efficiencies are 0.85, the same as in earlier studies [22,23]. Chacartegui et al. [14] investigated alternative cycles based on carbon dioxide for central receiver solar power plants using a turbine efficiency of 0.87. Cayer et al. [12] analyzed a carbon dioxide transcritical power cycle with a turbine efficiency of 0.8 using a low temperature source.

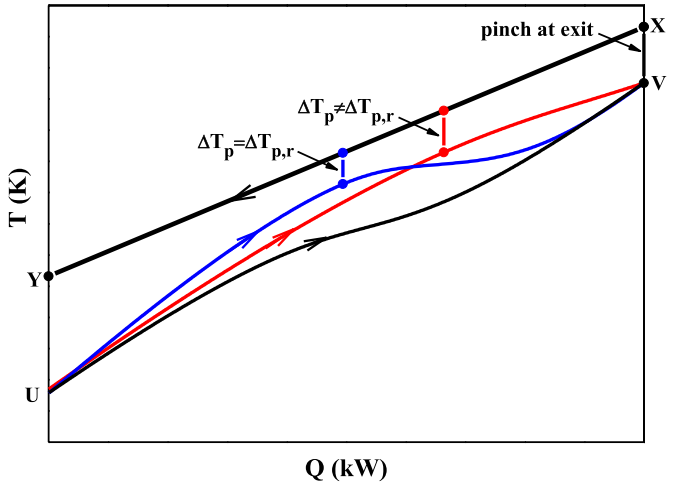

Fig. 2. *T*–*Q* curve for the flue gas and the organic fluid in the evaporator, the state parameters are $X(Q_a, T_{gas,in})$, $Y(0, T_{gas,out})$, $U(0, T_5)$ and $V(Q_a, T_1)$.

The algorithm assumes an initial P_1 then calculates the organic fluid enthalpy at the turbine inlet as $h_1 = h_1(P_1, T_1)$. The mass flow rate of the organic fluid is

$$Q_a = m_{ORC}(h_1 - h_5) \quad (3)$$

where m_{ORC} is the mass flow rate of the organic fluid. The pumping increases the organic fluid enthalpy by $h_5 = h_4 + W_p/m_{ORC}$, in which h_4 is the saturated liquid enthalpy at point 4 in Fig. 1.

In Fig. 2, the curve *UV* is given by

$$Q = m_{ORC}(h_{ORC} - h_5) \quad (4)$$

where h_{ORC} is dependent on P_1 and T_{ORC}. The pinch temperature difference between the flue gas and the organic fluid is based on $\Delta T_p = \min(T_{gas} - T_{ORC})$. The pinch location is either between the evaporator inlet and outlet or at the evaporator exit ($Q = Q_a$). An integrated-average temperature difference between the flue gas and the organic fluid in the evaporator is defined as

$$\Delta T_{ave} = \frac{\int_0^{Q_a} (T_{gas} - T_{ORC})\,dQ}{Q_a} \quad (5)$$

As shown in Fig. 2, even though the state parameters of $X(Q_a, T_{gas,in})$ $Y(0, T_{gas,out})$, $U(0, T_5)$ and $V(Q_a, T_1)$ are the same, different organic fluids yield different *T*–*Q* curves that result in different ΔT_{ave}. A protruded bow-shaped curve gives a smaller ΔT_{ave} with a better thermal match between the flue gas and the organic fluid. A concaved curve results in a larger ΔT_{ave} that has a bad thermal match between the flue gas and the organic fluid. There are three types of *UV* curve in Fig. 2.

(a) For a specific T_1, there is a supercritical pressure P_1 that forms the curve *UV* such that the pinch location is between the evaporator inlet and outlet. The pinch temperature difference satisfies the required value of $\Delta T_p = \Delta T_{p,r}$ (see the blue (in web version) curve in Fig. 2).

(b) For a specific T_1, there is a supercritical pressure P_1 that forms the curve *UV* such that the pinch location is between the evaporator inlet and outlet, but the pinch temperature difference does not satisfy the required value (e.g.,$\Delta T_p \neq \Delta T_{p,r}$, see the red (in web version) curve in Fig. 2).

(c) For a specific T_1, there is a supercritical pressure P_1 that forms the curve *UV* such that the pinch location is at the evaporator exit. The pinch temperature difference is $\Delta T_p = T_{gas,in} - T_1$, which may be different from the required value of $\Delta T_{p,r}$ (see the black curve in Fig. 2).

For mode a, P_1 is the first type solution corresponding to T_1. For mode c, P_1 is the second type solution corresponding to T_1. The ORC cannot operate at mode b because the pinch location does not occur at the evaporator exit nor satisfy the required value when the pinch location occurs between the evaporator inlet and outlet.

For a specific turbine inlet temperature ($T_1 \leq T_{1,max}$), the pressures are scanned to satisfy the pinch temperature difference requirement. The turbine inlet pressures are scanned from the critical pressure to the maximum pressure of 10.0 MPa. Fig. 3 illustrates the solution strategy for the search for P_1 corresponding to T_1. The operating parameters of the supercritical pressure ORCs are determined by changing the turbine inlet temperatures.

2.3. Thermal and exergy efficiencies

After all the state parameters in an ORC are determined, the pump power, turbine power and thermal efficiency are calculated as

$$W_p = m_{ORC}(h_5 - h_4) \quad (6)$$

$$W_t = m_{ORC}(h_1 - h_2) \quad (7)$$

$$\eta_{ORC} = \frac{W_t - W_p}{Q_a} \quad (8)$$

The computations of used exergy and exergy efficiency for each component are based on Mago et al. [24] and Tchanche et al. [25]. The detailed expressions are listed in Table 1. The exergy efficiency is defined as the used exergy divided by the available exergy. The system used exergy and available exergy are then the sum of the

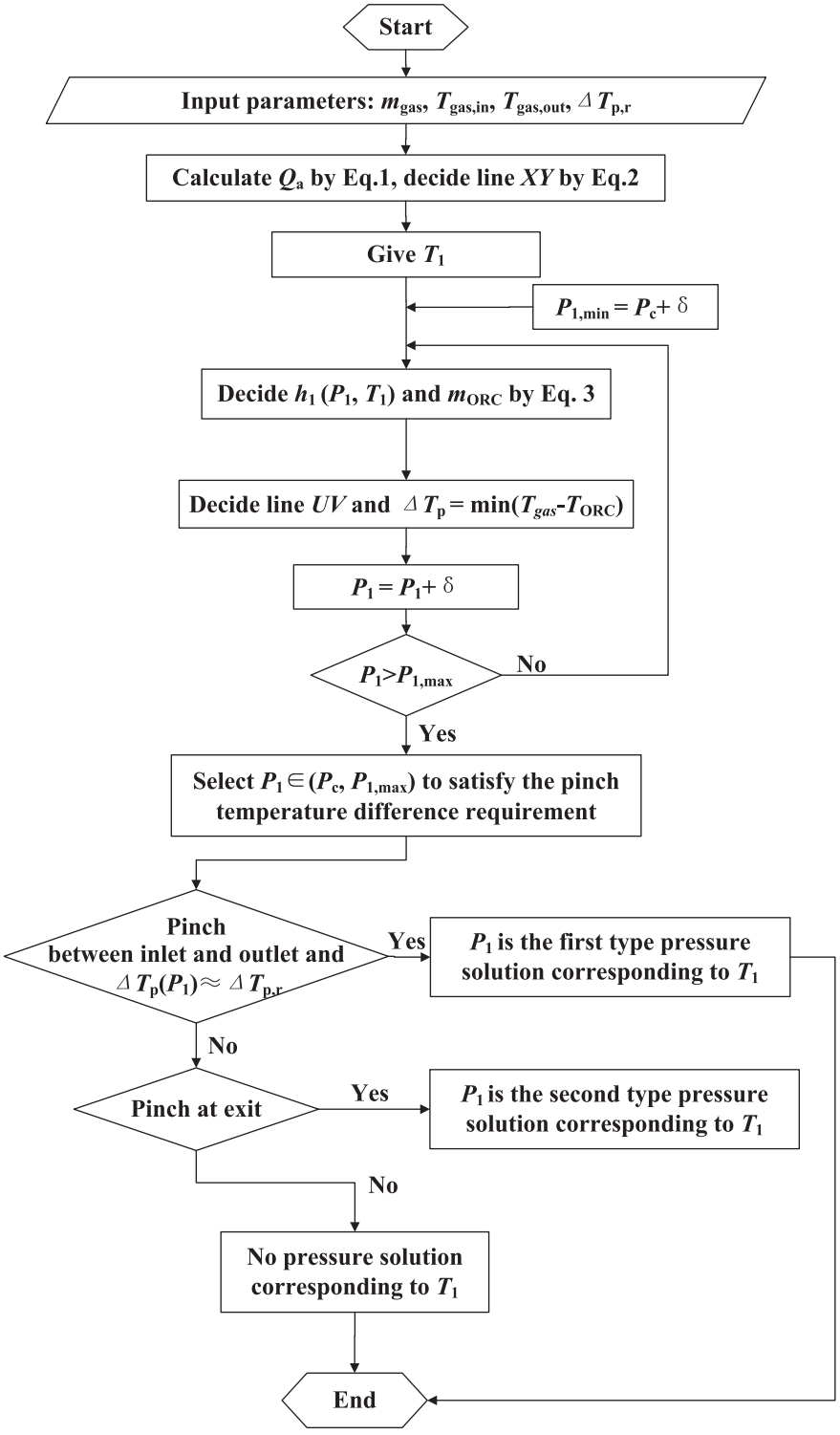

Fig. 3. Solution strategy for the relationship between P_1 and T_1.

Table 1
Exergy analysis for each ORC component.

Component	Evaporator	Turbine	Condenser	Pump
Schematic	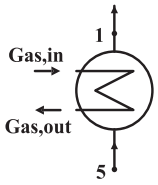	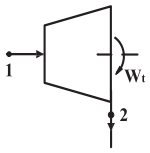	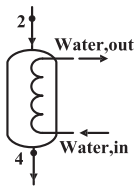	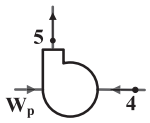
Used exergy	E_1-E_5	W_t	$E_{water,out}-E_{water,in}$	E_5-E_4
Available exergy	$E_{gas,in}-E_{gas,out}$	E_1-E_2	E_2-E_4	W_p

Table 2
Flue gas and cooling water conditions and turbine and pump isentropic efficiencies.

symbol	$T_{gas,in}$ (K)	$T_{gas,out}$ (K)	Q_a (kW)	$T_{water,in}$ (K)	$T_{water,out}$ (K)	T_4(K)	$\eta_{s,t}$	$\eta_{s,p}$
Value	423.15	343.15	1000	293.15	298.15	303.15	0.85	0.85

values for each component. The physical properties of the working fluids were computed using the NIST software. A Fortran code was written to do the computations shown in Fig. 3. The pressure of $P_0 = 0.1$ MPa and $T_0 = 293.15$ K were set as the reference state. The inlet and outlet temperatures of cooling water were 293.15 K and 298.15 K, respectively.

3. Results and discussion

3.1. Heat source and working fluids

The thermodynamic analysis calculates the useful power to be dependent on the flue gas exit temperature. In this study, the flue gas temperature was set to 423.15 K (150 °C) at the evaporator inlet and decreased to 343.15 K (70 °C) after heat was transferred to the organic fluid. The computations show that the maximum power occurs at a flue gas exit temperature of 70 °C. The power output was decreased when the flue gas exit temperature deviated from 70 °C. The flue gas mass flow rate is 12.34 kg/s so that the total heat released by the flue gas is 1.0 MW. Table 2 shows the parameters for the flue gas, cooling water and turbine and pump isentropic efficiencies.

The working fluids should be non-toxic, non-flammable, and environmentally friendly (low ODP (ozone depression potential) and GWP (global warming potential)). The effect of the critical temperature on the ORC was studied by selecting fluids with very different critical temperatures. The critical pressures could also be not too high or too low. The assumption in Section 2.2 is that the maximum operating pressure is 10.0 MPa. The supercritical pressure ORC must have a critical pressure of the organic fluid of less than 10.0 MPa. A low critical pressure of less than 1.0 MPa also reduces the power output because the turbine power is strongly influenced by the inlet pressure.

Three working fluids are used here. The first is R218 (also called Flutec PP30) which is a halogenated hydrocarbon with the chemical formula of C_3F_8. The second working fluid is R134a which is non-toxic, non-flammable, and non-corrosive with a large latent heat of evaporation and thermal decomposition at high temperature of 250 °C. Several studies [8,26,27] have recommended R134a as a good working fluid for ORCs. R134a has a moderate critical temperature between the other two organic fluids, which is the major reason to use R134a in this study. The third working fluid is R236fa, which is an HFC (hydrofluorocarbon) refrigerant. It is colorless, odorless and non-corrosive.

All three working fluids are non-flammable and have been recommended for ORCs [8,19,26–28]. Table 3 shows the key properties. The critical temperatures differ by more than 50 K.

3.2. ORC operating parameters

3.2.1. Flexible operating mode for low critical temperature fluids

For the flexible operating mode and any given turbine inlet temperature, any supercritical pressure at the turbine inlet has the pinch point at the evaporator exit ($Q = Q_a$). P_1 is the second type of pressure solution coupling the ORC with the heat source. Fig. 4a shows the pressures, P_1, versus temperatures, T_1, with R218 as the working fluid which has a critical temperature of 345.02 K (71.87 °C), significantly lower than the flue gas inlet temperature of 150 °C. The operating parameters of $P_1 \sim T_1$ form a rectangular regime with $T_1 \in [399.15\ K, T_{1,max}]$ and $P_1 \in [P_c, P_{1,max}]$, where $T_{1,max} = 413.15$ K and $P_{1,max} = 10.0$ MPa (the maximum pressure limit). Fig. 4b shows the pinch temperature difference versus the turbine inlet pressures for three turbine inlet temperatures of 399.15 K (minimum T_1), 406.15 K and 413.15 K (maximum T_1). The pinch temperature difference is constant and equals to $\Delta T_p = T_{gas,in} - T_1$ for any T_1.

Fig. 5a shows the T–Q curve for R218. For the higher turbine inlet temperature of $T_1(A) = T_1(B) = 413.15$ K, the maximum pressure of 10.0 MPa yields a quasi-linear T–Q curve due to the small change in the specific heats of the organic fluid with temperature. However, a lower pressure such as $P_1 = P_c + \delta = 2.65$ MPa results in a concaved bow-shaped T–Q profile due to the larger variations in the specific heat at low pressures. The minimum temperature of 399.15 K has a similar situation relative to the pressure effect as for 413.15 K. Fig. 5b shows the T–s diagrams with the four states of *A, B, C* and *D* marked. States *A* and *B* have the same turbine inlet temperature of 413.15 K, while states *C* and *D* have the same turbine inlet temperature of 399.15 K. States *A* and *D* have the same turbine

Table 3
Major property of the three working fluids.

Working fluid	Alternative name	MW (g/mol)	P_c (MPa)	T_c (K)	GWP_{100yr}	ODP
Octafluoropropane	R218	188.02	2.640	345.02	8830	0
1,1,1,2-Tetrafluoroethane	R134a	102.03	4.059	374.21	1430	0
1,1,1,3,3,3-Hexafluoropropane	R236fa	152.04	3.200	398.07	9650	0

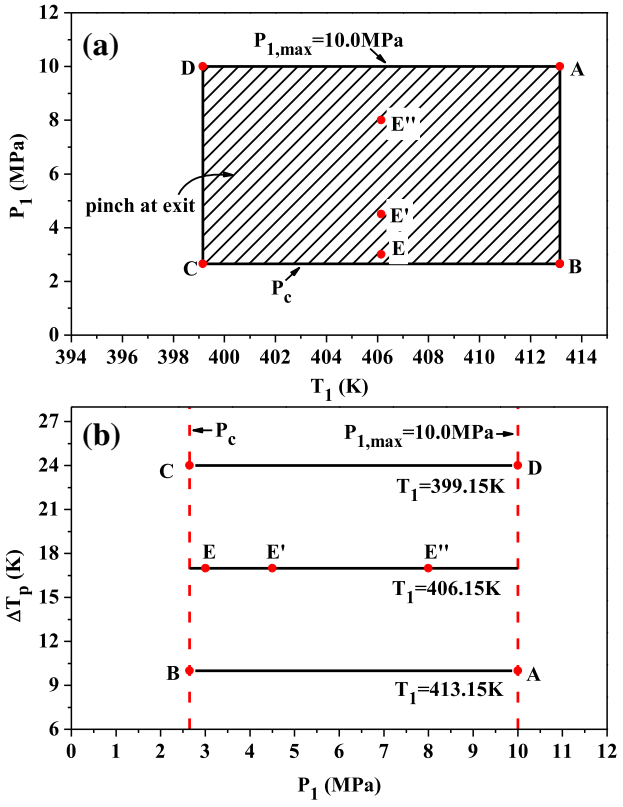

Fig. 4. The flexible operating mode (a: P_1 versus T_1; b: pinch temperature difference versus P_1. the work fluid is R218, *A* (413.15 K, 10.0 MPa), *B* (413.15 K , 2.65 MPa), *C* (399.15 K, 2.65 MPa), *D* (399.15 K , 10.0 MPa), *E* (406.15 K, 3.006 MPa), *E′* (406.15 K, 4.50 MPa), *E″* (406.15 K, 8.0 MPa)).

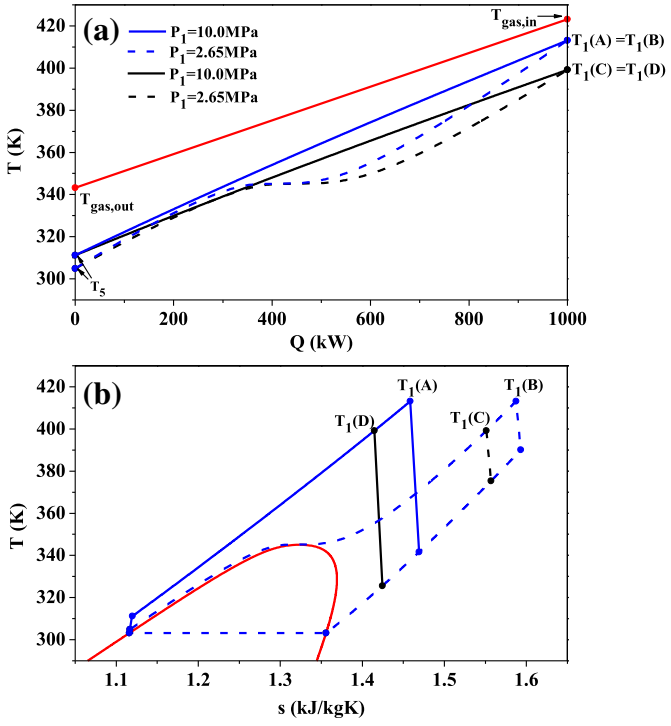

Fig. 5. *T*–*Q* curve and *T*–*s* diagram for R218 (pressures and temperatures at points *A*, *B*, *C* and *D* are identical to those in Fig. 4).

inlet pressure of 10.0 MPa (maximum limit) while states *B* and *C* have the same pressure of 2.65 MPa. The computed maximum thermal efficiency is $\eta_{th} = 0.107$ at state *A* and the secondary largest thermal efficiency is $\eta_{th} = 0.098$ at state *D*. States *B* and *C* have the smaller thermal efficiencies.

As shown in Fig. 5b, the turbine inlet temperature is significantly larger than the critical temperature. Thus, trapezoid cycles are formed in which the vapor is significantly superheated at the condenser inlet. There is a longer superheated vapor flow section in the condenser that reduces the condenser exergy efficiency. Therefore, the trapezoid cycle is not a good cycle and triangular cycle should be searched to improve the thermal performance [29].

3.2.2. *Bifurcated operating mode for moderate critical temperature fluids*

The bifurcated operating mode is so named because two turbine inlet pressures can be used with the same inlet temperature when an organic fluid has a moderate critical temperature. R134a is a representative fluid and P_1 is given by the first type pressure solution. The pinch location appears between the evaporator inlet and outlet. Fig. 6a illustrates the turbine inlet pressures versus temperatures. The pressures are in the range of 4.171–6.773 MPa for the temperatures in the range of 405.15–410.15 K. Two pressures (bifurcation) can be used with one temperature for T_1 in the narrow range of 405.15–406.15 K.

Fig. 6b shows the pressure (P_1) effect on the pinch temperature differences. The two limits of P_c and $P_{1,max} = 10.0$ MPa are marked. For a lower turbine inlet temperature such as $T_1 = 404.15$ K, the $\Delta T_p \sim P_1$ curve is above the required pinch temperature difference of $\Delta T_{p,r} = 10.0$ K, yielding no pressure solution for such T_1 (see the

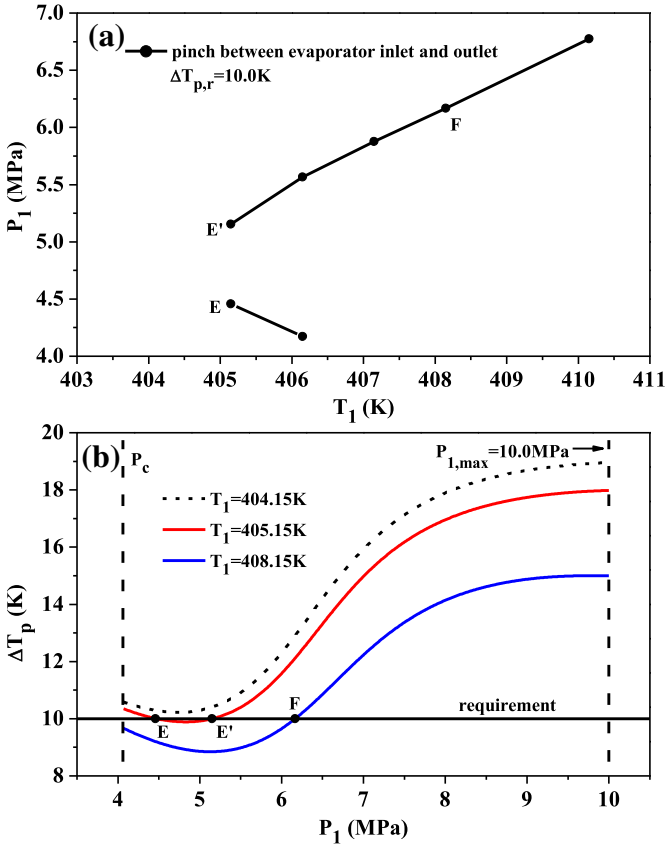

Fig. 6. Bifurcated operating mode (a: $P_1 \sim T_1$; b: pinch temperature differences versus P_1. The working fluid is R134a, *E* (405.15 K, 4.458 MPa), *E′* (405.15 K, 5.153 MPa), *F* (408.15 K, 6.167 MPa)).

dashed curve). The $\Delta T_p \sim P_1$ curve has two junctions with the required line of $\Delta T_{p,r} = 10.0$ K at $T_1 = 405.15$ K, forming two pressures of $P_{1,E} = 4.458$ MPa and $P_{1,E'} = 5.153$ MPa (see the red (in web version) curve). At larger T_1 such as $T_1 = 408.15$ K, the $\Delta T_p \sim P_1$ curve returns to a single pressure solution (one junction with the required line of $\Delta T_{p,r} = 10.0$ K, see the blue (in web version) curve).

Fig. 7a ~ b shows $T \sim Q$ and T–s curves for the two states of E and E' having the same temperature of 405.15 K. Both pressures of 4.458 MPa and 5.153 MPa satisfy the pinch temperature difference requirement of 10.0 K, but the pinch locations are slightly shifted. Fig. 7b shows the slight movement of the T–s curve to the left at the higher pressure of 5.153 MPa. Fig. 7c~d shows the $T \sim Q$ and T–s diagrams for $T_1 = 408.15$ K, at which only a single pressure, P_1, satisfies the pinch temperature difference requirement of 10.0 K. Comparing Figs. 5 and 7 shows that as the critical temperatures increase, the T–Q curves change from concaved-bow shape to protruded-bow shape, while the T–s diagrams change from the trapezoid cycle to the triangular cycle.

3.2.3. *Restricted operating mode for high critical temperature fluids*

The restricted operating mode is so called due to having only a single pressure for a specific temperature at the turbine inlet which occurs for high critical temperature fluids such as R236fa. The pinch location occurs between the evaporator inlet and outlet. Fig. 8a illustrates the pressures versus temperatures. Fig. 8b shows how the pinch temperature differences vary with the pressures. The pressure solution is obtained at the junction of the $\Delta T_p \sim P_1$ curve with the $\Delta T_{p,r} = 10.0$ K line. The pinch temperature differences sharply increase near the junction, beyond which they are less influenced by the pressures. In Fig. 8a, the operating conditions at points A and C are (399.15 K, 3.210 MPa) and (408.15 K, 3.848 MPa), respectively. Fig. 9 shows the T–Q and T–s diagrams with only a small difference between the two cycles. Fig. 9b shows that, because the fluid critical temperature approaches the flue gas inlet temperature, the T–s diagrams (black and blue (in web version) curves) almost coincide with the red (in web version) fluid T–s curve envelope, creating a triangular cycle that has good ORC thermal performance.

The expansion in the turbine depends not only on the fluid pressures and temperatures at the turbine inlet, but also on whether a dry fluid or wet fluid is used. Schuster et al. [13] investigated the efficiency optimization of supercritical ORCs. They noted that a fluid was acceptable when the vapor content at the turbine outlet was larger than 0.90 to avoid droplet erosion. Saleh et al. [7] investigated working fluids for low-temperature ORCs. They identified the exit vapor content of 0.96 for one cycle with R152a as the working fluid, which was acceptable for a practical cycle. However, the other cycles with R143a and R290 had exit vapor contents of 0.84 and 0.63, which are not recommended for real applications due to the unreasonably low exit vapor qualities [7].

Chen et al. [19] commented on the two-phase expansion issue. Even though their expansion went into the two-phase region, the flow leaving the turbine was still a dry fluid with a substantial superheat. For dry fluids, Goswami et al. [30] and Demuth [31,32] found that only extremely fine droplets (fog) were formed in the two-phase region with no liquid actually formed to damage the turbine before it started drying during the expansion. The flow at the turbine exit may be two-phase for a wet fluid. For a wet fluid such as water, Bakhtar et al. [33–37] found that the fluid first subcools and then nucleates to become a two-phase mixture. The formation and behavior of the liquid in the turbine create problems

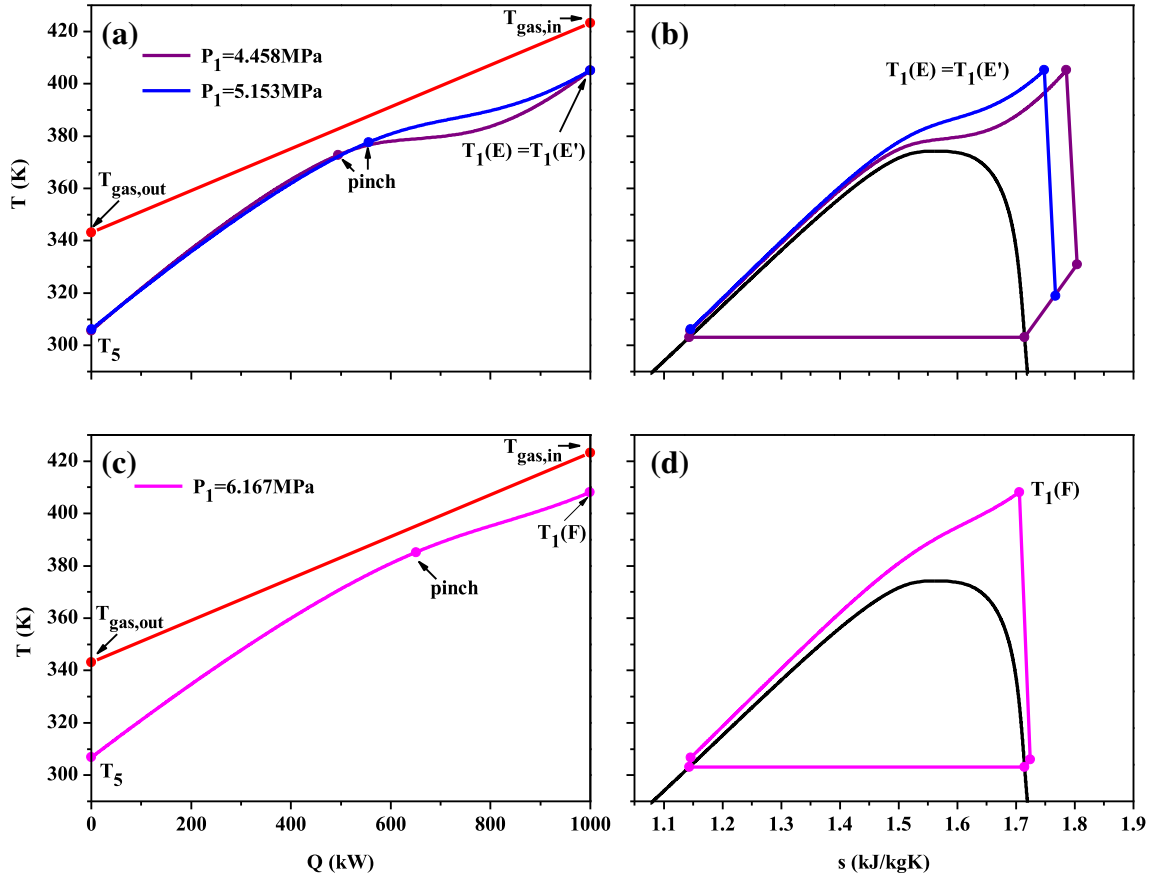

Fig. 7. T–Q curve and T–s diagram for R134a (the state parameters at points E, E' and F are identical to those in Fig. 6).

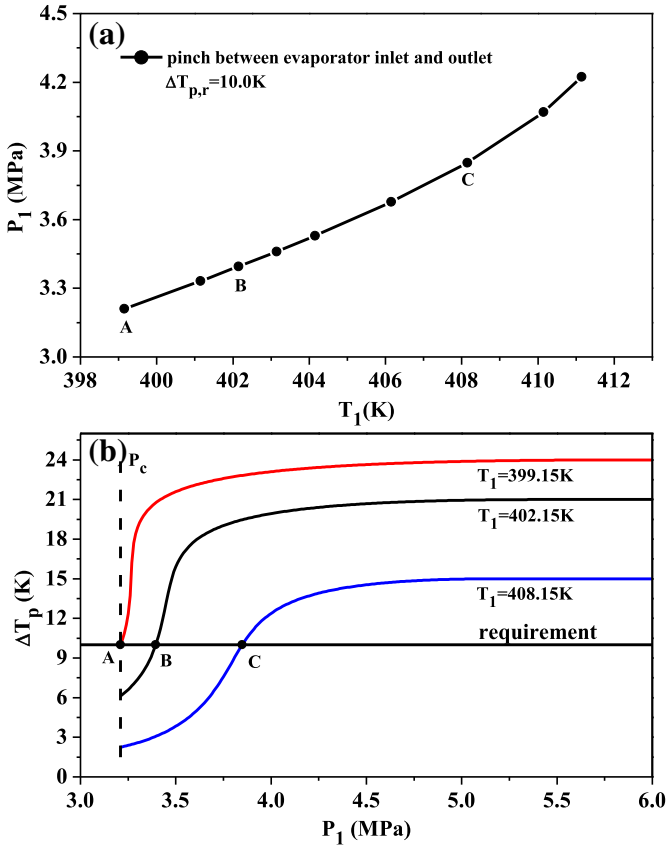

Fig. 8. Restricted operating mode (a: $P_1 \sim T_1$; b: pinch temperature differences versus P_1. The working fluid is R236fa, *A* (399.15 K, 3.210 MPa), *B* (402.15 K, 3.395 MPa), *C* (408.15 K, 3.848 MPa)).

that would lower the turbine performance. Alternatively, Demuth [31] found that the turbine performance is not degraded significantly when the expansion process passes into the wet region if no condensation occurs.

The expansion process shown in Fig. 9 is similar to those shown in Fig. 5a in Chen et al. [19]. Even though the flow enters the two-phase region during the expansion process, the fluid at the turbine outlet is still superheated due to the dry R236fa fluid. Dry fluids help to overcome or at least partially overcome the two-phase expansion problem. Thus, the cycles shown in Fig. 9 are acceptable.

3.3. Thermal and exergy efficiencies dependent on critical temperatures

Fig. 10 shows the mass flow rates of organic fluids, m_{ORC}, the thermal efficiencies, η_{ORC}, and the system exergy efficiencies, $\eta_{ex-e,sys}$, versus turbine inlet temperatures (T_1). R218, which operates with the flexible ORC operating mode, has a trapezoid distribution of the mass flow rates which are the largest among the three working fluids. R134a has the smallest mass flow rates with R236fa having the intermediate mass flow rates as shown in Fig. 10a. Fig. 10b shows that R236fa (the restricted operating mode) and R134a (the bifurcated operating mode) have the thermal efficiencies of about 13%, which are significantly larger than the efficiencies of 7–10% for R218.

R236fa and R134a have larger critical temperatures than R218. The *T*–*Q* curves of organic fluids behave protruded-bow shapes that approach the flue gas *T*–*Q* line. The pinch locations always occur between the evaporator inlet and outlet, yielding smaller integrated-average temperature difference in the evaporator, ΔT_{ave}, that result in higher evaporator exergy efficiencies. Mago et al. [24] noted that the evaporator accounts for the largest amount of exergy destroyed in an ORC. Al-Sulaiman et al. [5] performed energy and exergy analyses of a biomass trigeneration system using an ORC. Their study also revealed that the ORC evaporator contributed the majority of the exergy loss in the ORC. Increasing the evaporator exergy efficiency significantly improves the ORC performance. This explains why R134a and R236fa with larger evaporator exergy efficiencies have larger thermal efficiencies as shown in Fig. 10b–c than R218.

Table 4 further verifies the above analysis. T_1 is 406.15 K. Pressures in the range of P_1 = 2.650–10.0 MPa can match T_1 (flexible operating mode) for R218. The integrated-average temperature differences, ΔT_{ave}, are in the range of 31.16–23.25 K, which are the largest among the three working fluids. The evaporator and system exergy efficiencies are the lowest with the smallest system thermal efficiencies of 7.0–10.3%.

R134a and R236fa have the integrated-average temperature differences of 17–20 K, with significantly larger evaporator and system exergy efficiencies than R218. The thermal efficiencies range from 12.8% to 13.4%, significantly larger than R218. Generally, the efficiencies are similar for R134a and R236fa. The difference between the two fluids is the bifurcated pressure solution for R134a and the single pressure solution for R236fa.

3.4. Explanation of the observed phenomena

3.4.1. Pinch location dependent on the critical temperature of fluids

This section explains the phenomena reported in Sections 3.2 and 3.3. Now Fig. 2 and Eqs. (2) and (4) are recalled. The slopes of the *T*–*Q* curve for the flue gas and the organic fluid are

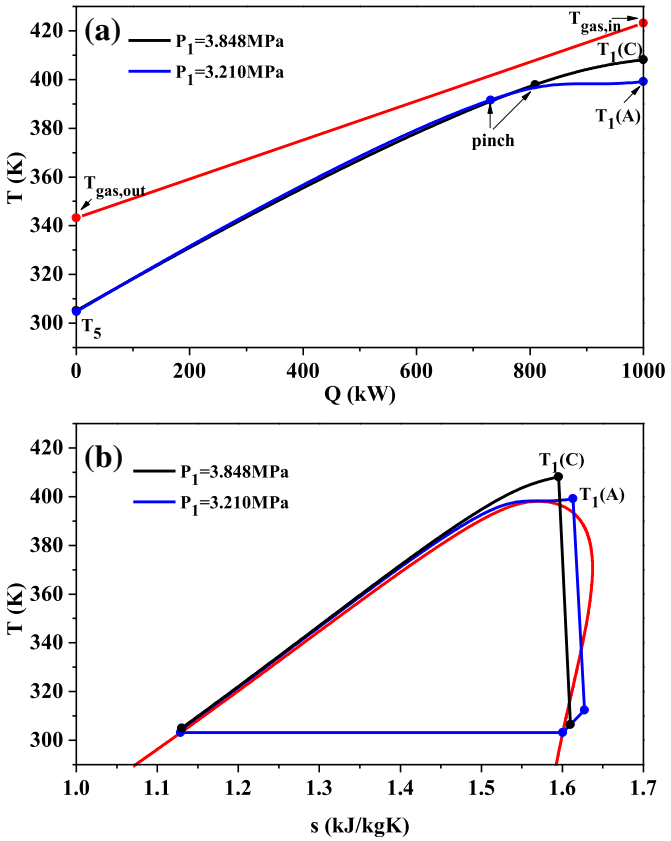

Fig. 9. *T*–*Q* curve and *T*–*s* diagram for R236fa (the state parameters at points *A* and C are identical to those in Fig. 8).

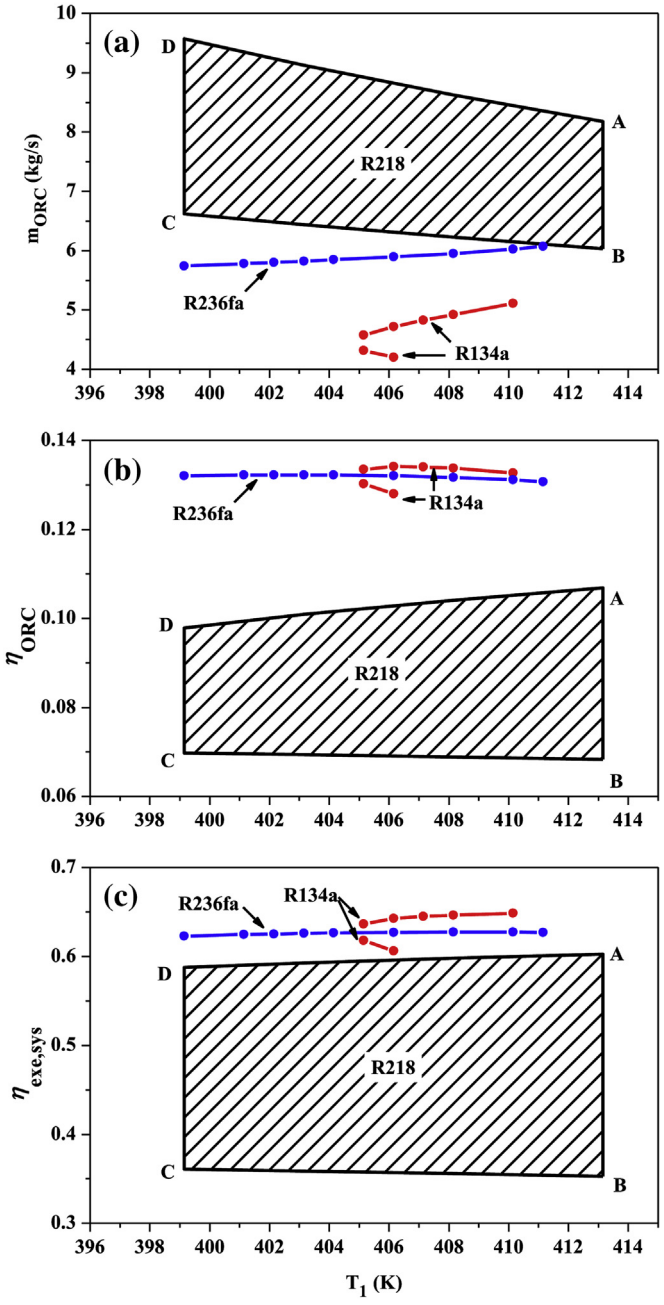

Fig. 10. Mass flow rates, system thermal efficiencies and exergy efficiencies with R218, R134a and R236fa.

$$\frac{\partial T_{gas}}{\partial Q} = \frac{1}{m_{gas}C_{p,gas}} = k_{gas} \tag{9}$$

$$\frac{\partial T_{ORC}}{\partial Q} = \frac{1}{m_{ORC}C_{p,ORC}} = k_{ORC} \tag{10}$$

The temperature difference and its slope are defined as

$$\Delta T = T_{gas} - T_{ORC}, \quad \frac{\partial(\Delta T)}{\partial Q} = k_{gas} - k_{ORC} \tag{11}$$

To search for the pinch location, the following equation is considered:

$$\frac{\partial(\Delta T)}{\partial Q} = 0 \tag{12}$$

Equation (12) requires that $k_{gas} = k_{ORC}$. The $\Delta T = (T_{gas} - T_{ORC}) \sim Q$ curve satisfying the criterion of $k_{gas} = k_{ORC}$ has stagnation points but these might be maximum or minimum points. For the present application, k_{gas} is equal to 0.08 K/kW. Fig. 11a shows k_{gas} and k_{ORC} versus organic fluid temperatures in the evaporator, in which $T_1 = 405.15$ K and $P_1 = 4.458$ MPa with R134a as the working fluid. k_{ORC} has two junctions with $k_{gas} = 0.08$ K/kW line to generate two stagnation points of M and N. Fig. 11b shows the $\Delta T \sim T_{ORC}$ curve.

The pseudocritical temperature, T_{pc}, is the temperature at which the specific heat attains maximum at a specific supercritical pressure [38]. T_{pc} is varied in terms of pressures. Fig. 11 shows that T_M is slightly smaller than T_{pc}. M is the minimum ΔT point since $\partial(\Delta T)/\partial Q < 0$ at $T = T_M^-$ and $\partial(\Delta T)/\partial Q > 0$ at $T = T_M^+$. Similarly, N is the maximum ΔT point. Thus M is the minimum temperature difference point along the evaporator flow length ($0 < Q < Q_a$) where Eq. (12) is satisfied. Q_M is the heat received from the heat source at point M in the $T \sim Q$ curve. The pinch location can be found by comparing ΔT_M and ΔT_{exit} (temperature different at the evaporator exit, point V in Fig. 11). The pinch is at point M if $\Delta T_M < \Delta T_{exit}$ (such as shown in Fig. 11b). Otherwise, the pinch is at the evaporator exit if $\Delta T_M > \Delta T_{exit}$.

The effect of the critical temperatures on the pinch location was analyzed. Fig. 12 shows the specific heats of R218, R134a and R236fa at supercritical pressures. Three C_p curves are given for each fluid. Each curve shows the $C_p \sim T$ relation at a specific pressure. C_p is infinite at P_c and T_c, but it has a large finite value at a supercritical pressure P and its pseudocritical temperature T_{pc}. For each fluid, the minimum pressure was 0.01 MPa larger than P_c. The other two pressures were chosen to have similar $C_{p,max}$ at T_{pc} as the other two fluids. Fig. 12 shows that a lower T_c fluid has a lower T_{pc} to reach the same $C_{p,max}$ than a higher T_c fluid. Fig. 11 shows that T_M approaches T_{pc}. Thus, T_M decreases with decreasing T_c. In other words, point M can be far from the evaporator entrance with a high T_c fluid.

Fig. 13 shows $C_{p,ORC}$, k_{ORC} and T–Q curve for R218 and R134a. Two factors that influence ΔT_p and its location are k_{ORC} in the evaporator entrance region ($T_{ORC} < T_M$ or $Q < Q_M$) and the point M location at which $k_{gas} = k_{ORC}$.

Fig. 13 shows that R134a (higher T_c) has larger k_{ORC} in the evaporator entrance region. In addition, M' is far from the evaporator entrance (see the red (in web version) curves for R134a). These two factors ensure a smaller temperature difference at M' ($\Delta T_{M'}$). R218 (lower T_c) has smaller k_{ORC} in the evaporator entrance region and M is close to the evaporator entrance. These make a larger temperature difference at M (ΔT_M). Comparing $\Delta T_{M'}$ and ΔT_M with ΔT_{exit} suggests that high critical temperature fluids such as R134a have a large possibility that the pinch is located between the evaporator inlet and outlet and low critical temperature fluids such as R218 locate the pinch at the evaporator exit.

The pinch location at the evaporator exit creates a larger integrated-average temperature difference due to a larger enclosed

Table 4
ORC performance parameters with R218, R134a and R236fa at $T_1 = 406.15$ K $m_{gas} = 12.34$ kg/s, $T_{gas,in} = 423.15$ K and $T_{gas,out} = 343.15$ K

Working fluids	T_c (K)	P_1 (MPa)	ΔT_{ave} (K)	$\eta_{exe,eva}$	$\eta_{exe,sys}$	η_{ORC}
R218	345.02	2.650–10.0	31.16–23.25	0.701–0.779	0.357–0.597	0.070–0.103
R134a	374.21	4.171	20.26	0.810	0.607	0.128
		5.567	17.71	0.830	0.643	0.134
R236fa	398.07	3.677	19.17	0.812	0.628	0.132

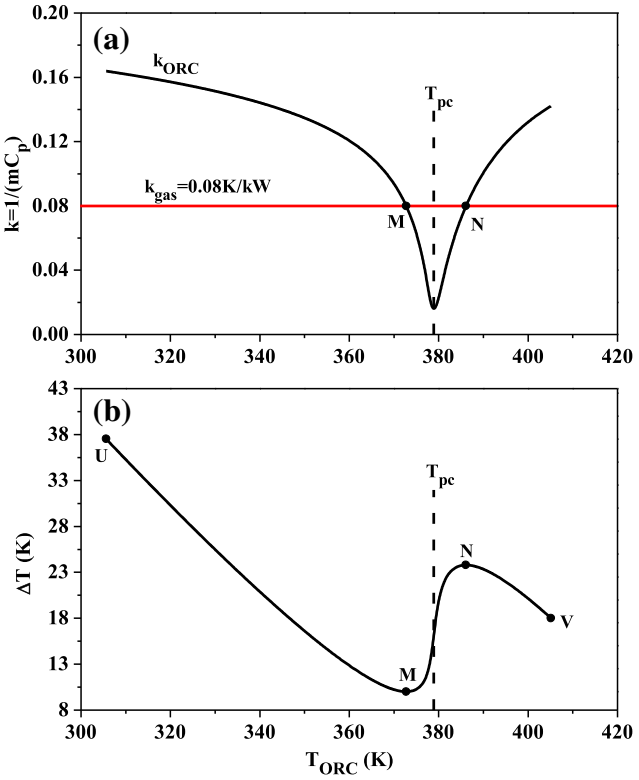

Fig. 11. k_{ORC} and ΔT versus organic fluid temperatures with R134a as the working fluid.

area formed by the T–Q curves for the flue gas and the organic fluid. This causes smaller evaporator and system exergy efficiencies as for R218 with its lower critical temperature (see Figs.4 and 5). Alternatively, the pinch location between the evaporator inlet and outlet results in a smaller integrated-average temperature difference, increasing the evaporator and system exergy efficiencies as for R134a and R236fa with their higher critical temperatures (see Figs.6–9).

3.4.2. Bifurcated pressure solution for R134a and single pressure solution for R236fa

Integration of Eq. (12) yields the temperature difference at point M ($k_{gas} = k_{ORC}$):

$$\Delta T_M = (T_{gas} - T_{ORC})_M = k_{gas} Q_M - \int_0^{Q_M} k_{ORC} dQ + T_{gas,out} - T_5 \tag{13}$$

Equation (13) is correct because k_{gas} is constant for a given heat source. Since the last two terms of the right side of Eq. (13) are given, the integral $\int_0^{Q_M} k_{ORC} dQ$ should be large so that ΔT_M can be smaller than ΔT_{exit}. Three situations satisfy the requirement that the pinch is located between the evaporator inlet and outlet:

- larger k_{ORC} in the evaporator entrance region and later appearance of point M at which $k_{gas} = k_{ORC}$ (i.e., larger Q_M)
- larger k_{ORC} in the evaporator entrance region and earlier appearance of point M at which $k_{gas} = k_{ORC}$ (i.e., smaller Q_M)

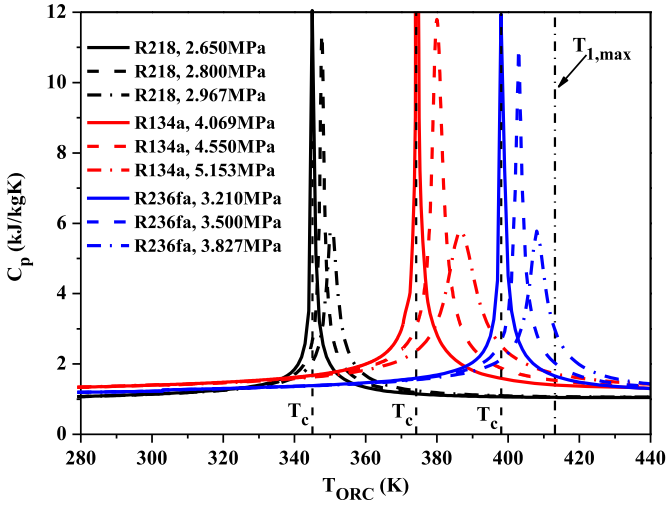

Fig. 12. Specific heats versus temperatures for the three working fluids.

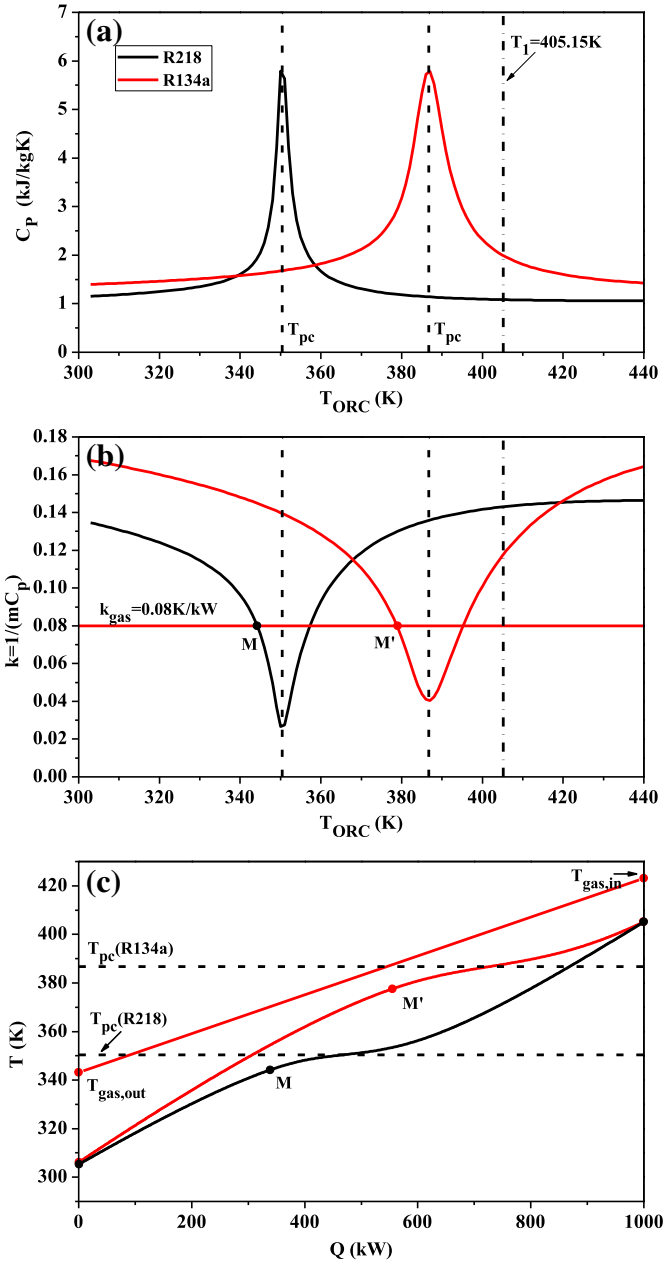

Fig. 13. C_p, k_{ORC} and T–Q curves for R134a and R218 at $T_1 = 405.15$ K ($T_{pc} = 350.4$ K, $P_1 = 2.96$ MPa for T–Q curve of R218; $T_{pc} = 386.7$ K, $P_1 = 5.153$ MPa for T–Q curve of R134a).

- smaller k_{ORC} in the evaporator entrance region and later appearance of point M at which $k_{gas} = k_{ORC}$ (i.e., larger Q_M).

Fig. 14 explains the bifurcated pressure solution for R134a. The two pressures of 4.458 MPa and 5.153 MPa can both be used with $T_1 = 405.15$ K. Fig. 14a shows the specific heats versus fluid temperatures. Fig. 14b shows that $P_1 = 4.458$ MPa has larger k_{ORC} than $P_1 = 5.153$ MPa in the evaporator entrance region. However, point M for $P_1 = 4.458$ MPa appears earlier than point M' for $P_1 = 5.153$ MPa as seen in Fig. 14b. Thus, the bifurcated pressure solution is caused by the following reason:

- The pinch location at point M for $P_1 = 4.458$ MPa is due to larger k_{ORC} in the evaporator entrance region and earlier appearance of point M;

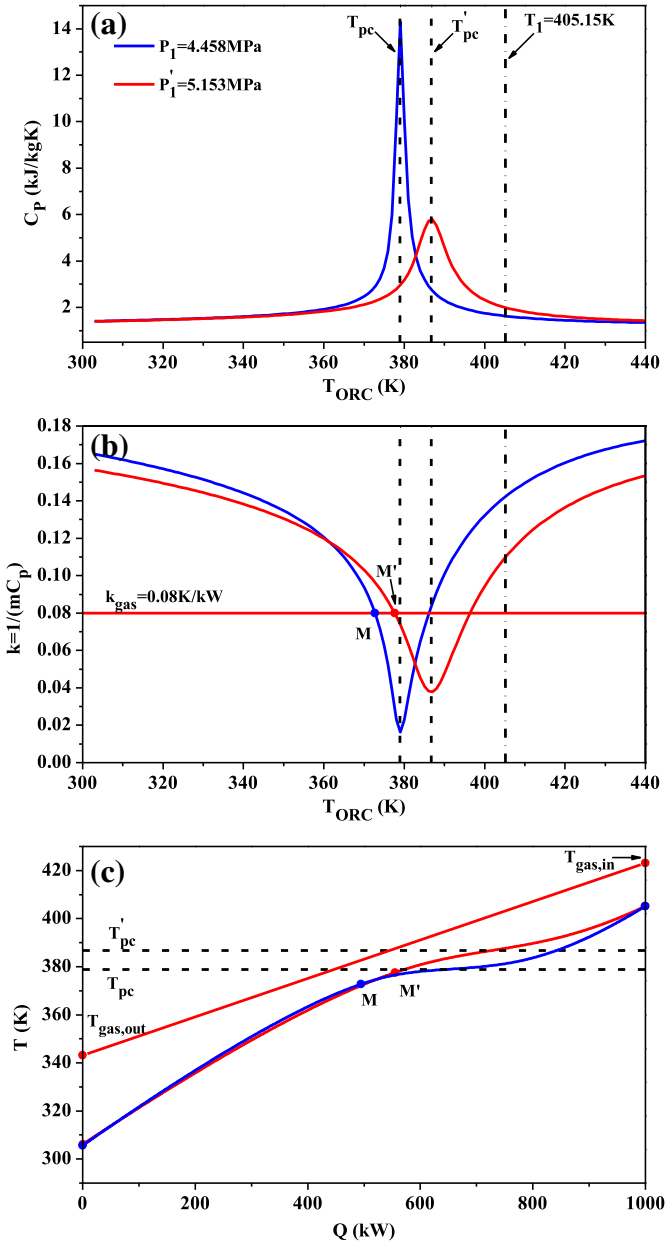

Fig. 14. Explanation of the bifurcated pressure solution for R134a (both $P_1 = 4.458$ MPa ($T_{pc} = 378.19$ K) and 5.153 MPa ($T_{pc} = 386.70$ K) are the pressures adapting to $T_1 = 405.15$ K).

- The pinch location at point M' for $P_1 = 5.153$ MPa is due to smaller k_{ORC} in the evaporator entrance region and later appearance of point M'.

Finally, the single pressure solution with R236fa was explained. This can be done by comparing k_{ORC} for R134a and R236fa (see Fig. 15). Fig. 15a shows that different pressures cause significantly different k_{ORC} in the evaporator entrance region. Meanwhile, different pressures also cause different locations of point M at which $k_{gas} = k_{ORC}$. This is the reason of the bifurcated pressure solution for R134a.

Fig. 15b shows that different pressures cause obviously different k_{ORC} in the evaporator entrance region. But pressures have little influence on the intersection points at which $k_{ORC} = k_{gas}$. Thus, R236fa has only a single pressure solution.

3.5. Heat transfer consideration

Many articles have dealt with the heat transfer issues at supercritical pressures [38], beginning as early as the 1930s. In the 1950s, the concept of using supercritical “steam” to increase the thermal efficiency of fossil-fired power plants became an attractive option. Currently, the use of supercritical “steam” in fossil-fired power plants is the largest industrial application of fluids at supercritical pressures. Near the end of the 1950s and at the beginning of the 1960s, several studies investigated the potential of using supercritical water as a coolant in nuclear reactors. The USA and former USSR (Union of Soviet Socialist Republics) extensively studied supercritical heat transfer from the 1950s until the 1980s. Research was focused on circular water-cooled tube flow geometry. A comparison of selected supercritical water heat transfer correlations has shown that their results may differ from one another by more than 200%. Thus, there is still a need for a reliable, accurate and wide range supercritical water heat transfer correlation [38].

The ORC design needs accurate heat transfer coefficients at supercritical pressures with organic fluids as the working fluids. Karellas et al. [39] investigated the influence of supercritical ORC parameters on plate heat exchanger design. The key scientific issue is the significant change in the physical properties versus temperature at supercritical pressures. Some well-known heat transfer coefficients in heat transfer handbooks may not be valid for ORC heat transfer design. Karellas et al. [39] recommended dividing the heat exchanger into a set of elementary areas assuming equal enthalpy difference. Results using 1000 partitions of a heat exchanger are used as a reference. Their study showed the heat transfer surface area increased with increasing pressure.

Even though many studies have been performed on supercritical water heat transfer for nuclear reactor applications [40], supercritical CO_2 heat transfer for heat pump applications [41], and some supercritical organic fluid heat transfer for ORC applications [39], these studies are not sufficient to design a real supercritical pressure ORC plant at this stage. Future studies should include (1) fundamental studies of supercritical organic fluid heat transfer; (2) experimental studies and correlations of heat transfer coefficients of supercritical organic fluids at various flow geometries, operating parameters and inclination angles, etc. Finally, an investigation of real-scale supercritical ORC applications is also vital for the actual exploitation of this promising technology. Only after those fields are thoroughly investigated, final and reliable conclusions can be drawn [39].

4. Comparison with other studies

Usually, the thermal efficiency and useful power are two independent objective parameters. This study proposed a new method to couple an ORC with the heat source. The thermal efficiency and useful power are combined into one objective parameter due to the fixed heat

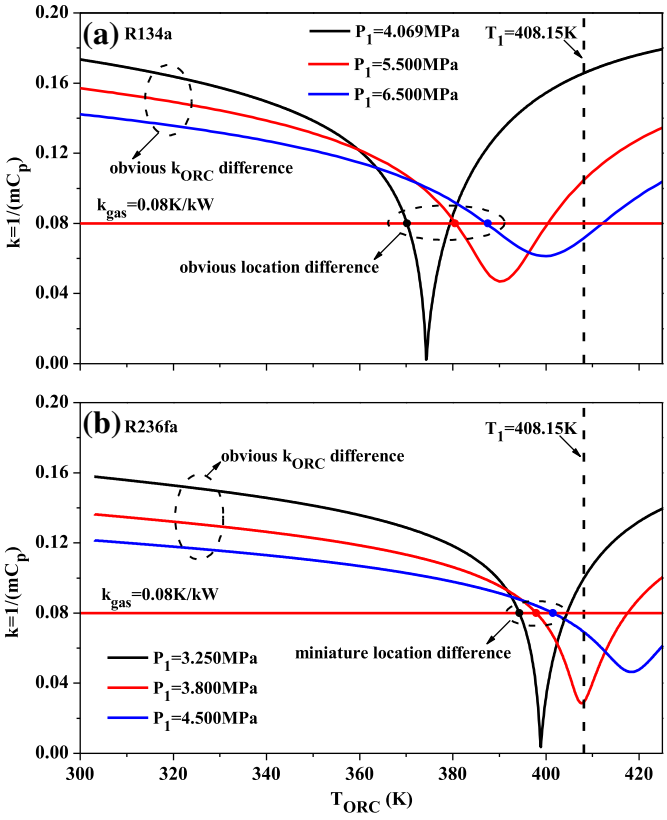

Fig. 15. Explanation of the bifurcated pressure solution for R134a and single pressure solution for R236fa (only one pressure of $P_1 = 3.848$ MPa adapts to $T_1 = 408.15$ K for R236fa).

received from the heat source. Thus, one expects a desired waste heat recovery degree. The new method guides engineers in designing a waste heat driven ORC with a discharged flue gas temperature as low as possible. Based on the method, three operating modes were identified.

Flexible operating mode: If a low critical temperature fluid (such as R218 with its T_c 78 K lower than $T_{gas,in} = 423.15$ K) is used, the pinch location at the evaporator exit results in a concaved-bow shaped $T \sim Q$ curve with a large integrated-average temperature difference between the flue gas and the organic fluid. A set of turbine inlet pressures can be used with a given turbine inlet temperature, forming the rectangular operating regime for P_1 as a function of T_1. The exergy and thermal efficiencies are low. This mode is not recommended for ORC applications.

Bifurcated operating mode: Moderate critical temperature fluids such as R134a cause the pinch to be located between the evaporator inlet and outlet. The protruded $T \sim Q$ curve yields smaller integrated-average temperature difference. One or two pressures can be used with a specific turbine inlet temperature. The exergy and thermal efficiencies are relatively high.

Restricted operating mode: This mode occurs when the fluid critical temperature approaches the flue gas inlet temperature. This is similar to the bifurcated operating mode, except that only a single pressure can be used with a given turbine inlet temperature. The bifurcated and restricted operating modes are preferable for ORC designs.

This study provides the principle for selection of working fluids for supercritical pressure ORCs. Different heat source temperatures need different working fluids. Qualitatively, the fluid critical temperature should approach the inlet temperature of the heat source. A low critical temperature that is 78 K less than the flue gas temperature is not recommended. This explains why CO_2 is not a good working fluid in supercritical pressure ORCs, because it has a critical temperature of 31.0 °C, which is significantly lower than the heat source temperature, even for a 100 °C flue gas heat source.

Quantitatively, the term $\int_0^{Q_M} k_{ORC} dQ$ in Eq. (13) should be large so that $\Delta T_M < \Delta T_{exit}$ to ensure that the pinch is located between the evaporator inlet and outlet, which can be a criterion for the working fluid selection.

Classical thermodynamic analyses of ORC systems do not fix the flue gas outlet temperature [7,9], but design a T–s cycle based on the flue gas inlet temperature. The slope of the T–Q line for the heat carrier fluid is used to search for a suitable outlet temperature of the heat source. The present method differs from the classical thermodynamic analysis. Table 5 lists the supercritical pressure ORC studies for heat source inlet temperature of about 150 °C [2,22,42,43] in which the heat source, optimal thermal efficiency and working fluid are listed case by case. Vélez et al. [42] used CO_2 as the working fluid with a thermal efficiency of only 7.3%, which is significantly lower than those in this study shown in Table 4 due to the low critical temperature of CO_2. Zhang & Jiang [22] and Astolfi et al. [43] also used R134a as the working fluid with optimized thermal efficiencies of 12.7% and 13.6%. Our results listed in Table 4 have thermal efficiencies in the range of 12.8–13.4%, which are very close to those in the previous studies [22,43] using R134a. Note that the optimal thermal efficiency does not mean the largest useful power output in the literature since the two objective parameters differ.

5. Conclusions

The major findings are summarized as follows.

- A design method was proposed to couple an ORC with the heat source.

Table 5
Supercritical pressure ORC studies in the literature.

Ref.	Heat source	Recommended working fluids	Optimized η_{ORC}	Comments
[2]	Geothermal fluid, inlet temperature of 150 °C, mass flow of 20 kg/s	R227ea	10.28%	The highest specific net power output with varied turbine inlet temperatures was found at the fixed pinch temperature difference and condensing temperature.
[22]	Geothermal fluid, inlet temperature of 150 °C, mass flow of 1 kg/s	R134a (only)	12.70%	The operating pressure was optimized to maximize the thermal efficiency.
[42]	Isothermal heat source at 140 °C	CO_2 (only)	7.3%	The optimum pressure was assumed to be the average of the pressures giving the maximum energy efficiency and net specific work with a turbine inlet temperature of 120 °C.
[43]	Geothermal fluid, inlet temperature of 150 °C, outlet temperature of 70 °C with a flow rate of 100 kg/s	R134a	13.60%	The net power from the geothermal brine was maximized assuming that the thermal input was the maximum heat available.

- An integrated-average temperature difference between the heat carrier fluid and the organic fluid in the evaporator is used to evaluate the evaporator and system exergy efficiencies.
- The three types of operating modes for organic fluids with critical temperatures that vary by more than 50 K are (1) the flexible operating mode where a range of pressures can be used with a specific turbine inlet temperature for low critical temperature fluids; (2) the bifurcated operating mode with one or two pressures can be available with a specific turbine inlet temperature for moderate critical temperature organic fluids; (3) and the restricted operating mode with a single pressure can be used with a given turbine inlet temperature for high critical temperature fluids.
- The pinch location between the evaporator inlet and outlet or at the evaporator exit depends on k_{ORC} in the evaporator entrance region and the point M location at which $k_{ORC} = k_{gas}$. The integral $\int_0^{Q_M} k_{ORC} dQ$ should be large so that the temperature difference at point M (see Eq. (13)) can be smaller than that at the evaporator exit. This ensures that the pinch is not at the evaporator exit and can be used a design criterion for supercritical pressure ORCs.
- The critical temperatures influence the pinch location, integrated-average temperature difference, exergy and thermal efficiencies. Organic fluids with critical temperatures approaching the inlet temperature of the heat source yield pinch located between the evaporator inlet and outlet, causing large exergy and thermal efficiencies.

Acknowledgments

This work was supported by the Natural Science Foundation of China of International cooperation project (51210011), the National Basic Research Program of China (2011CB710703), the Beijing Science and Technology Program (Z111109055311097), and the 111 project (B12034).

References

[1] Hung TC, Shai TY, Wang SK. A review of organic Rankine cycles (ORCs) for the recovery of low grade waste heat. Energy 1997;22(7):661–7.
[2] Vetter C, Wiemer HJ, Kuhn D. Comparison of sub- and supercritical Organic Rankine Cycles for power generation from low-temperature/low-enthalpy geothermal wells, considering specific net power output and efficiency. Appl Therm Eng 2013;51(1–2):871–9.
[3] Heberle F, Brüggemann D. Exergy based fluid selection for a geothermal Organic Rankine Cycle for combined heat and power generation. Appl Therm Eng 2010;30(11–12):1326–32.
[4] Guo T, Wang HX, Zhang SJ. Selection of working fluids for a novel low-temperature geothermally-powered ORC based cogeneration system. Energy Convers Manag 2011;52(6):2384–91.
[5] Al-Sulaiman FA, Dincer I, Hamdullahpur F. Energy and exergy analyses of a biomass trigeneration system using an organic Rankine cycle. Energy 2012;45(1):975–85.
[6] Hung TC, Wang SK, Kuo CH, Pei BS, Tsai KF. A study of organic working fluids on system efficiency of an ORC using low-grade energy sources. Energy 2010;35(3):1403–11.
[7] Saleh B, Koglbauer G, Wendland M, Fischer J. Working fluids for low-temperature organic Rankine cycles. Energy 2007;32(7):1210–21.
[8] Lakew AA, Bolland O. Working fluids for low-temperature heat source. Appl Therm Eng 2010;30(10):1262–8.
[9] Lai NA, Wendland M, Fischer J. Working fluids for high-temperature organic Rankine cycles. Energy 2011;36(1):199–211.
[10] Chen H, Goswami DY, Rahman MM, Stefanakos EK. A supercritical Rankine cycle using zeotropic mixture working fluids for the conversion of low-grade heat into power. Energy 2011;36(1):549–55.
[11] Karellas S, Schuster A. Supercritical fluid parameters in organic Rankine cycle applications. Int J Thermodyn 2008;11(3):101–8.
[12] Cayer E, Galanis N, Desilets M, Nesreddine H, Roy P. Analysis of a carbon dioxide transcritical power cycle using a low temperature source. Appl Energy 2009;86(7–8):1055–63.
[13] Schuster A, Karellas S, Aumann R. Efficiency optimization potential in supercritical Organic Rankine Cycles. Energy 2010;35(2):1033–9.
[14] Chacartegui R, Escalona JMM, Sánchez D, Monje B, Sánchez T. Alternative cycles based on carbon dioxide for central receiver solar power plants. Appl Therm Eng 2011;31(5):872–9.
[15] Arslan O, Yetik O. ANN based optimization of supercritical ORC-binary geothermal power plant: simav case study. Appl Therm Eng 2011;31(17–18):3922–8.
[16] Zhang S, Wang H, Guo T. Performance comparison and parametric optimization of subcritical Organic Rankine Cycle (ORC) and transcritical power cycle system for low-temperature geothermal power generation. Appl Energy 2011;88(8):2740–54.
[17] Baik YJ, Kim M, Chang KC, Kim SJ. Power-based performance comparison between carbon dioxide and R125 transcritical cycles for a low-grade heat source. Appl Energy 2011;88(3):892–8.
[18] Vélez F, Segovia JJ, Martín MC, Antolín G, Chejne F, Quijano A. A technical, economical and market review of organic Rankine cycles for the conversion of low-grade heat for power generation. Renew Sustain Energy Rev 2012;16(6):4175–89.
[19] Chen HJ, Goswami DY, Stefanakos EK. A review of thermodynamic cycles and working fluids for the conversion of low-grade heat. Renew Sustain Energy Rev 2010;14(9):3059–67.
[20] Tchanche BF, Lambrinos G, Frangoudakis A, Papadakis G. Low-grade heat conversion into power using organic Rankine cycles – a review of various applications. Renew Sustain Energy Rev 2011;15(8):3963–79.
[21] Guo WQ. Thinking of establishing security system for natural gas heating in Beijing. Dist Heat 2013;2:10–4 [Chinese version].
[22] Zhang FZ, Jiang PX. Thermodynamic analysis of a binary power cycle for different EGS geofluid temperatures. Appl Therm Eng 2012;48(15):476–85.
[23] Franco A, Villani M. Optimal design of binary cycle power plants for water-dominated, medium-temperature geothermal fields. Geothermics 2009;38(4):379–91.
[24] Mago PJ, Srinivasan KK, Chamra LM, Somayaji C. An examination of exergy destruction in organic Rankine cycles. Int J Energy Res 2008;32(10):926–38.
[25] Tchanche BF, Lambrinos G, Frangoudakis A, Papadakis G. Exergy analysis of micro-organic Rankine power cycles for a small scale solar driven reverse osmosis desalination system. Appl Energy 2010;87(4):1295–306.
[26] Sauret E, Rowlands AS. Candidate radial-inflow turbines and high-density working fluids for geothermal power systems. Energy 2011;36(7):4460–7.
[27] Gu Z, Sato H. Performance of supercritical cycles for geothermal binary design. Energy Convers Manag 2002;43(7):961–71.
[28] Rayegan R, Tao YX. A procedure to select working fluids for Solar Organic Rankine Cycles (ORCs). Renew Energy 2011;36(2):659–70.
[29] DiPippo R. Ideal thermal efficiency for geothermal binary plants. Geothermics 2007;36(3):276–85.
[30] Goswami DY, Hingorani S, Mines G. A laser-based technique for particle sizing to study two-phase expansion in turbines. J Sol Energy Eng 1991;113(3):211–8.
[31] Demuth OJ. Analyses of mixed hydrocarbon binary thermodynamic cycles for moderate temperature geothermal resources. Idaho; 1981.
[32] Demuth OJ. Preliminary assessment of condensation behavior for hydrocarbon-vapor expansions which cross the saturation line near the critical point. Idaho; 1983.
[33] Bakhtar F, Mashmoushy H, Buckley JR. On the performance of a cascade of turbine rotor tip section blading in wet steam. Part 1: generation of wer steam of prescribed droplet sizes. Proc Inst Mech Eng C Mech Eng Sci 1997;211(7):519–29.
[34] Bakhtar F, Mashmoushy H, Jadayel OC. On the performance of a cascade of turbine rotor tip section blading in nucleating steam. Part 3: wake traverses. Proc Inst Mech Eng C Mech Eng Sci 1997;211(8):639–48.
[35] Bakhtar F, Mashmoushy H, Jadayel OC. On the performance of a cascade of turbine rotor tip section blading in wet steam. Part 2: surface pressure distributions. Proc Inst Mech Eng C J Mech Eng Sci 1997;211(7):531–40.
[36] Bakhtar F, Henson RJK, Mashmoushy H. On the performance of a cascade of turbine rotor tip section blading in wet steam. Part 5: theoretical treatment. Proc Inst Mech Eng C J Mech Eng Sci 2006;220(4):457–72.
[37] Bakhtar F, Rassam SY, Zhang G. On the performance of a cascade of turbine rotor tip section blading in wet steam. Part 4: droplet measurements. Proc Inst Mech Eng C J Mech Eng Sci 1999;213(4):343–53.
[38] Pioro I, Mokry S, Draper S. Specifics of thermophysical properties and forced-convective heat transfer at critical and supercritical pressures. Rev Chem Eng 2011;27(3–4):191–214.
[39] Karellas S, Schuster A, Leontaritis AD. Influence of supercritical ORC parameters on plate heat exchanger design. Appl Therm Eng 2012;33-34:70–6.
[40] Pioro I, Duffey RB. Experimental heat transfer in supercritical water flowing inside channels (survey). Nucl Eng Des 2005;235(12):2407–30.
[41] Jiang PX, Zhao CR, Shi RF, Chen Y, Ambrosini W. Experimental and numerical study of convection heat transfer of CO_2 at super-critical pressures during cooling in small vertical tube. Int J Heat Mass Transf 2009;52(21–22):4748–56.
[42] Vélez F, Segovia J, Chejne F, Antolín G, Quijano A, Martín MC. Low temperature heat source for power generation: exhaustive analysis of a carbon dioxide transcritical power cycle. Energy 2011;36(9):5497–507.
[43] Astolfi M, Xodo L, Romano MC, Macchi E. Technical and economical analysis of a solar–geothermal hybrid plant based on an Organic Rankine Cycle. Geothermics 2011;40(1):58–68.